NeuroImage: Clinical 23 (2019) 101880

Contents lists available at ScienceDirect

NeuroImage: Clinical

journal homepage: www.elsevier.com/locate/ynicl

Diffusion tensor imaging reveals changes in microstructural integrity along compressed nerve roots that correlate with chronic pain symptoms and motor deficiencies in elderly stenosis patients

Hughes S.W.[a], Hellyer P.J.[b,c], Sharp D.J.[b], Newbould R.D.[d], Patel M.C.[e], Strutton P.H.[a,*]

[a] The Nick Davey Laboratory, Division of Surgery, Imperial College London, UK
[b] Computational, Cognitive and Clinical Neuroimaging Laboratory, Division of Brain Sciences, Imperial College London, London, UK
[c] Department of Bioengineering, Imperial College London, UK
[d] Imanova, Ltd, UK
[e] Imaging Department, Imperial College Healthcare NHS Trust, Charing Cross Hospital, London, UK

ARTICLE INFO

Keywords:
Neuropathic pain
Spinal nerve
Entrapment
DTI
Neurophysiology
Age

ABSTRACT

Age-related degenerative changes in the lumbar spine frequently result in nerve root compression causing severe pain and disability. Given the increasing incidence of lumbar spinal disorders in the aging population and the discrepancies between the use of current diagnostic imaging tools and clinical symptoms, novel methods of nerve root assessment are needed. We investigated elderly patients with stenosis at L4-L5 or L5-S1 levels. Diffusion tensor imaging (DTI) was used to quantify microstructure in compressed L5 nerve roots and investigate relationships to clinical symptoms and motor neurophysiology. DTI metrics (i.e. FA, MD, AD and RD) were measured at proximal, mid and distal segments along compressed (i.e. L5) and intact (i.e. L4 or S1) nerve roots. FA was significantly reduced in compressed nerve roots and MD, AD and RD were significantly elevated in the most proximal segment of the nerve root studied. FA was significantly correlated with electrophysiological measures of root function: minimum F-wave latency and peripheral motor conduction time (PMCT). In addition, FA along the compressed root also correlated with leg pain and depression score. There was also a relationship between RD and anxiety, leg pain and disability score and AD correlated with depression score. Taken together, these data show that DTI metrics are sensitive to nerve root compression in patients with stenosis as a result of age-related lumbar degeneration. Critically, they show that the changes in microstructural integrity along compressed L5 nerve roots are closely related to a number of clinical symptoms associated with the development of chronic pain as well as neurophysiological assessments of motor function. These inherent relationships between nerve root damage and phenotype suggest that the use DTI is a promising method as a way to stratify treatment selection and predict outcomes.

1. Introduction

Up to 40% of people will experience radicular low-back pain symptoms at some point during their lifetime and it is most prevalent in the aging population, occurring in approximately 50% of 60–69 year olds (Kalichman et al., 2009; NICE, 2016). Progressive, age-related spinal degeneration including a reduced intervertebral disk height, ligamentum flavum hypertrophy and facet joint hypertrophy can cause stenosis within the lateral recess and intervertebral foramen (Melancia et al., 2014). This can result in neuropathic pain radiating along the sciatic nerve (radiculopathy) as a consequence of compression, irritation and/or inflammation of exiting spinal nerves.

Up to 75% of cases of stenosis cause entrapment of the transiting or exiting L5 nerve root in the lateral recess or foramen (Orita et al., 2016). Radiculopathy often produces pain that radiates over the L5 dermatome and weakness of the tibialis anterior (TA) muscle associated with severe functional impairment. Currently, the primary diagnostic indicators include magnetic resonance imaging (MRI) and nerve conduction velocity (NCV) studies (Verwoerd et al., 2013). MRI provides key information regarding the extent of the stenosis. However current approaches to MRI reporting do not provide quantitative information regarding the extent of nerve root compression and discrepancies

* Corresponding author at: The Nick Davey Laboratory, Human Performance Group, Division of Surgery, Department of Surgery and Cancer, Faculty of Medicine, Imperial College London, W6 8RF, UK.
E-mail address: p.strutton@imperial.ac.uk (P.H. Strutton).

https://doi.org/10.1016/j.nicl.2019.101880
Received 3 September 2018; Received in revised form 15 April 2019; Accepted 25 May 2019
Available online 28 May 2019

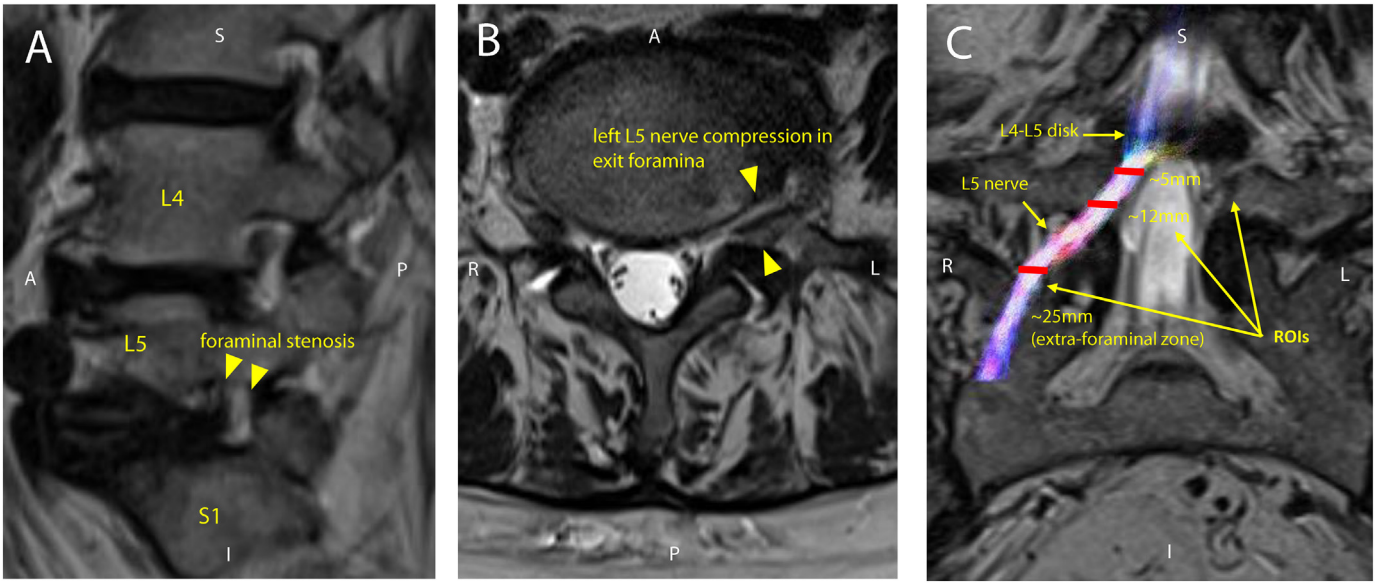

Fig. 1. A) Schematic showing the affected (red L5) and unaffected (green L4 or S1) nerve roots B) Sagittal T2-weighted MRI showing left L5 nerve compression in the intervertebral foramen C) schematic showing region of interest (ROI) placement along an L5 nerve root with respect to distance below the L4-L5 disc. Note that ROIs are shown on coronal view for clarity of position along the nerve root.

Table 1
Patient demographics and clinical details. F: female. M: male. VAS; visual analogue scale (0, no pain; 10, maximum pain). HADS: hospital anxiety depression scale (0, no depression; 21, maximum depression). ODI: Oswestry Low Back Disability Questionnaire (0, no disability; 100, maximum disability). RMDQ: Roland Morris Disability Questionnaire (0, no disability; 24, maximum disability).

ID	Age	Gender	Leg pain Symptoms	Pain duration	Average leg pain VAS	HADS depression	HADS anxiety	ODI (%)	RMDQ
1	66	F	Ache	1 year	8.00	7	2	64	12
2	70	F	Shooting	1–4 years	7.00	15	14	48	12
3	80	F	Shooting	1 year	6.00	6	9	45	11
4	63	F	Ache	1–4 years	6.67	7	7	24	13
5	72	F	Sharp/shooting	6 months	5.67	5	9	53	18
6	74	M	Shooting	> 10 years	5.33	10	11	48	18
7	63	M	Sharp	1–4 years	8.00	9	11	54	16
8	57	M	Shooting	1–4 years	6.67	3	2	22	8
9	68	F	Stabbing/shooting	1–4 years	9.00	11	7	31.4	6
10	68	F	Sharp	5–10 years	7.67	11	9	46.6	17
11	47	M	Shooting	5–10 years	8.33	4	7	46	15
12	71	M	Ache	5–10 years	7.00	5	2	28.8	12
13	77	M	Ache, stabbing	5–10 years	10.00	10	12	60	23
14	53	M	Sharp	1–4 years	4.33	8	4	17.5	9
15	68	F	Ache	> 10 years	8.00	5	3	66.6	14
16	66	F	Ache/sharp	5–10 years	8.50	15	19	62	18
17	53	F	Ache	1–4 years	9.33	2	8	38	8
18	64	F	Burning, sharp	1 year	7.67	1	3	16	7
19	58	F	Ache	5–10 years	5.33	8	4	55.5	13
20	64	M	Shooting	> 10 years	6.33	6	3	14	1
Mean (SD)	65.1 (8.3)	–	–	–	7.2 (1.5)	7.4 (3.8)	7.3 (4.6)	42.1 (16.9)	12.6 (5.1)

between symptoms, MRI features and NCV tests are common (El Barzouhi et al., 2016).

Diffusion tensor imaging (DTI) has found wide clinical utility in neurological disorders (Hellyer et al., 2013; Sharp et al., 2014). It is potentially very informative in patients with spinal nerve root compression as it provides a means by which to quantify the degree of nerve damage (Balbi et al., 2011; Kitamura et al., 2012; Kanamoto et al., 2016; Eguchi et al., 2016b; Eguchi et al., 2016a; Oikawa et al., 2015; Eguchi et al., 2011). Through the use of the diffusion tensor applied to diffusion weighted images, quantitative values such as fractional anisotropy (FA), axial diffusivity (AD), radial diffusivity (RD) and mean diffusivity (MD) may be determined. These diffusion measures are sensitive to changes in the microstructural integrity of compressed nerve roots; including degree of axonal loss, demyelination and oedema (Takahashi et al., 2003; Rydevik et al., 1991; Rydevik et al., 1984). Recent studies have reported reduced FA and elevated MD values along damaged spinal nerves associated with the diagnosis of lumbar disc herniation or foraminal stenosis. Hence the method has the potential to increase the diagnostic sensitivity of MRI for radiculopathy caused by lateral recess or foraminal narrowing (Kitamura et al., 2012; Kanamoto et al., 2016; Eguchi et al., 2016b; Eguchi et al., 2016a). However, given the discrepancies between conventional imaging and patient reported symptoms, it is surprising that the inherent relationships between DTI values derived along compressed nerve roots and phenotypes associated with chronic pain have yet to be investigated.

In our previous work, we have validated the use of DTI for studying spinal nerve structure in healthy subjects. Critically, we have demonstrated that microstructural integrity assessed by DTI is strongly associated with related neurophysiological measures such as F-wave latency and M-wave amplitude (Chiou et al., 2017). However, a factor not

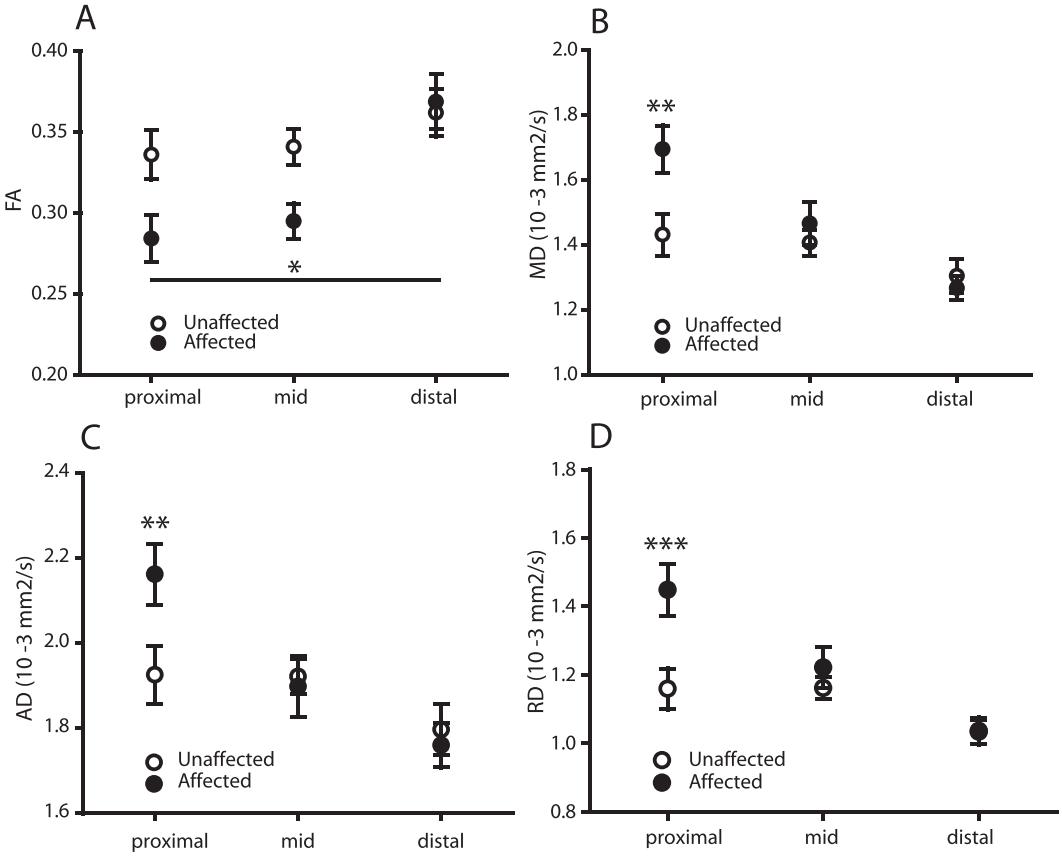

Fig. 2. Altered microstructural integrity along compressed L5 nerve roots. A) Reduced FA in affected versus unaffected nerve roots. At the proximal end of the compressed nerve root there was an increased in B) MD C) AD and D) RD. Affected nerves = left or right L5 based on radiological confirmation; unaffected nerves = left or right L4 or S1 based on radiological confirmation. Data are expressed as mean ± SEM; 2-way RM ANOVA with Holm-Sidak multiple comparison post-hoc tests; *- $p < 0.05$; **- $p < 0.01$; ***- $p < 0.001$; $N = 20$.

examined in any detail thus far is how the structural integrity or damage to nerve roots relate to neurophysiological measurements and clinical symptoms in elderly patients with nerve root compression in the exit foramina. Therefore, in this work we apply the novel imaging and data processing methods developed in our previous work to elderly patients in order to quantify the degree of compression along compressed L5 nerve roots as they traverse the intervertebral foramina. We then explore relationships between these discreet measures of microstructural integrity and clinical and functional phenotypes. Specifically, we assess the differences in microstructural integrity along affected (i.e. L5) and unaffected (i.e. L4 or S1) nerve roots in elderly patients with foraminal stenosis and determine the relationship between the diffusion data and neurophysiological responses from the TA muscle as well as clinical symptoms associated with the development of chronic pain. Our hypotheses were that there would be pathological changes in diffusion values measured along compressed nerve roots when compared to an unaffected level and that these changes in microstructural integrity would be associated with the presence of chronic pain symptoms, motor impairment and electrophysiological abnormalities.

2. Materials and methods

2.1. Participants

25 elderly patients with lateral recess and/or foraminal stenosis (11 female; mean ± SD age 65.1 ± 8.4 years) were recruited from Imperial College London and University College London NHS Trusts. Patients were included if they had 1) radiological evidence of either unilateral or bilateral L5 nerve root compression as result of spinal degeneration at the L4-L5 or L5-S1 levels (i.e. reduced disc height, ligamentum flavum hypertrophy, facet joint hypertrophy), diagnosed by a consultant radiologist (author MP), 2) symptoms of radiculopathy following the dermatomal pattern of L5 and 3) at least one unaffected nerve root at either L4 or S1. Patients were excluded from the study if they had previously received spinal decompression surgery or if they met any of the exclusion criteria for MRI (i.e. metal implants), cardiac pacemaker, previous brain injury, history of epilepsy or fits, neurosurgery, neurological disorders, psychological disorders (Rossi et al., 2011). Following screening, 20 patients with unilateral or bilateral L5 nerve root compression with intact L4 or S1 nerve roots were used in the analysis. All procedures were approved by the local research ethics committee. All subjects gave informed written consent in accordance with the principles of the declaration of Helsinki.

2.2. MRI data acquisition

All MRI data were collected using a 3 T Siemens Verio clinical MRI scanner (Siemens Healthcare, Erlangen Germany). Subjects were imaged supine using an 11 cm local loop coil centred over the intervertebral disc between L5 and S1 in combination with 2 elements of the phased-array spine coil to maximise the signal-to-noise ratio in the lumbar roots. Coil positioning was verified by initial localizer scans. Structural imaging for the radiological review by a consultant radiologist to confirm evidence of lumbar nerve compression included sagittal T1-weighted (T1w) and T2-weighted (T2w) turbo spin echo (TSE), coronal T2w TSE, as well as a multislab T2w TSE angled axial to L3-L4, L4-L5 and L5-S1 vertebral discs. Diffusion weighted images (DWI) were acquired with b = 800 s/mm^2 using a twice-refocused

Table 2
Relationship between FA, MD, AD and RD and the battery of neurophysiological measures. Results from multiple linear regression analyses between the diffusion metrics across all ROIs and neurophysiological responses measured at the TA muscle. AD: mean diffusivity, CMCT: central motor conduction time, FA, fractional anisotropy, MD: mean diffusivity, MEP: motor evoked potential, PMCT: peripheral motor conduction time, RD: radial diffusivity, ROI: region of interest. N = 20. * = significant correlation following correction for multiple comparisons using false detection rate (FDR).

Diffusion metric ROI	MEP amplitude	MEP latency	F-wave latency	PMCT	CMCT
FA					
Proximal	r = 0.15	r = −0.07	r = −0.36	r = −0.39	r = 0.37
	p = 0.65	p = 0.83	p = 0.16	p = 0.13	p = 0.23
Mid	r = 0.41	r = −0.14	r = −0.55	r = −0.54	r = 0.52
	p = 0.90	p = 0.96	p = 0.02*	p = 0.03*	p = 0.09
Distal	r = 0.21	r = −0.22	r = 0.67	r = −0.02	r = −0.52
	p = 0.51	p = 0.49	p = 0.79	p = 0.93	p = 0.08
MD					
Proximal	r = −0.81	r = 0.10	r = 0.13	r = 0.15	r = −0.15
	p = 0.80	p = 0.76	p = 0.62	p = 0.56	p = 0.63
Mid	r = −0.10	r = −0.13	r = 0.47	r = 0.35	r = −0.46
	p = 0.075	p = 0.70	p = 0.06	p = 0.17	p = 0.13
Distal	r = −0.61	r = 0.21	r = −0.16	r = 0.08	r = 0.25
	p = 0.04	p = 0.52	p = 0.54	p = 0.75	p = 0.44
AD					
Proximal	r = −0.13	r = 0.17	r = −0.01	r = 0.06	r = 0.01
	p = 0.68	p = 0.59	p = 0.99	p = 0.83	p = 0.99
Mid	r = −0.20	r = −0.03	r = 0.45	r = 0.35	r = −0.37
	p = 0.53	p = 0.92	p = 0.07	p = 0.17	p = 0.23
Distal	r = −0.56	r = 0.36	r = −0.07	r = 0.18	r = 0.14
	p = 0.06	p = 0.25	p = 0.80	p = 0.48	p = 0.67
RD					
Proximal	r = −0.17	r = 0.13	r = 0.07	r = 0.11	r = −0.04
	p = 0.59	p = 0.68	p = 0.78	p = 0.67	p = 0.90
Mid	r = −0.33	r = −0.02	r = 0.28	r = 0.19	r = −0.01
	p = 0.30	p = 0.96	p = 0.28	p = 0.46	p = 0.97
Distal	r = 0.22	r = 0.55	r = −0.01	r = 0.14	r = 0.25
	p = 0.50	p = 0.06	p = 0.98	p = 0.59	p = 0.43

diffusion preparation, an inverted slice select gradient on the refocusing pulses for improved fat saturation (Nagy and Weiskopf, 2008), and a 2D EPI readout. Forty 2.5 mm thick adjacent slices of a 100 × 256 mm field of view (FOV) were collected with TE = 92 ms, TR = 9 s, 50 × 128 resolution with readout bandwidth of 1562 Hz per pixel, giving a resolution of 2.0 × 2.0 × 2.5 mm. Saturation bands were placed superiorly and inferiorly to imaging slab to reduce flow and off-resonance excitation artefacts. 64 non-collinear directions interspersed with a b = 0 measurement after every 16 directions were collected resulting in 68 acquisitions in 10 m:21 s (Chiou et al., 2017).

2.3. Neurophysiological measurements

2.3.1. Recording

Electromyographic (EMG) recordings were obtained bilaterally from the target muscles predominantly innervated by the affected nerve root in the patients; tibialis anterior (TA) for the L5 and soleus for the S1. Pairs of Ag/AgCl electrodes (self-adhesive, 2 cm diameter, CareFusion, UK) were positioned parallel to the muscle fibre orientation. A ground electrode was placed over the left lateral malleolus. For TA, electrodes were positioned at 1/3 way along a line between the head of the fibula and the superior aspect of the medial malleolus. Participants were additionally asked to contract the target muscles by ankle dorsiflexion to confirm that the electrodes were located on the most prominent muscle bulk. EMG data were filtered (10–1000 Hz), amplified (1000×; Iso-DAM, World Precision Instruments, UK) and sampled at 2 kHz using a Power 1401 data acquisition system and Signal v5 software (Cambridge Electronic Design [CED], UK) connected to a computer for subsequent offline analysis.

2.3.2. Transcranial magnetic stimulation (TMS)

TMS was delivered to the motor cortex using a non-navigated Magstim 200^2 mono-phasic stimulator (The Magstim Company Ltd., UK) connected to a figure-of-eight coil (wing outer diameter 10 cm), positioned over the approximate location of primary motor cortex at a site which elicited a maximal motor evoked potential (MEP) in the contralateral target muscle, the hot-spot.

2.3.3. Experimental procedures

Measurements were conducted while participants were seated in an armchair with torso supported by the backrest and feet strapped securely on a wood plate on the floor. Three brief (~2 s) maximum voluntary contractions (MVC), with at least 10 s rest between contractions, were recorded from each target muscle; strong verbal encouragement was provided throughout. The mean rectified EMG over 500 ms during each of the three MVCs was calculated and averaged and 10% of this value was displayed continuously on a screen as visual feedback for participants during all TMS measurements.

2.3.4. Corticospinal excitability

Measurements were performed on each target muscle separately and while participants maintained contraction levels at 10% MVC of the target muscle (Hess et al., 1987; Nicotra et al., 2013). Active motor threshold (AMT) was established for each target muscle, which was defined as the lowest intensity of TMS that evoked visible MEPs in at least three of six consecutive trials. Motor evoked potentials (MEPs) were elicited by TMS and a stimulus response curve of MEP amplitude was constructed. Stimulus intensities started at 10% below the AMT and were increased in 10% steps of AMT until the intensity reached to the maximal device output (or twice AMT, whichever was the lower). Intensities were randomised and six MEPs at each intensity were recorded. TMS pulses were given every 8 s with several periods of rest given to participants between trials to avoid muscle fatigue.

2.3.5. M-wave and F-waves

Measurements were conducted while participants were seated in an armchair and torso supported by a backrest. A maximal motor response (M_{max}) and F-waves were measured following supramaximal stimuli via

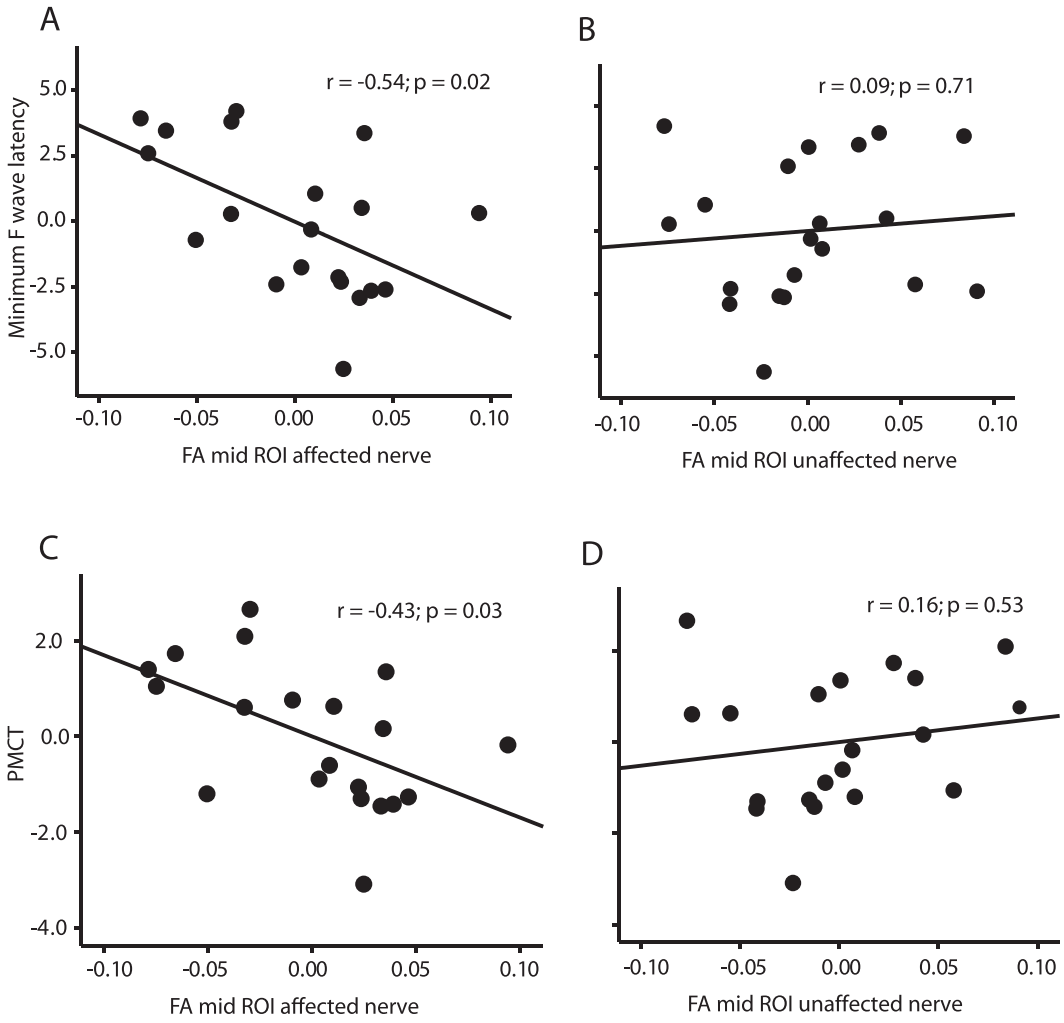

Fig. 3. Relationship between fractional anisotropy (FA) of affected and unaffected nerve roots and neurophysiological measurements obtained from the tibialis anterior (TA). Partial regression plots showing A) FA measured at the mid-part of the nerve correlated with minimum F-wave latency and C) peripheral motor conduction time (PMCT) when measured from the affected but not the unaffected (B and D) nerve roots. $N = 20$.

a cathode to the common peroneal nerve around the fibular head (Digitimer DS7, Digitimer UK, 500 -μs pulse duration). The anode was placed over the patella on the stimulated side. Five M_{max} at the same intensity were recorded. An intensity of 120% of the intensity used to elicit M_{max} was delivered at 1 Hz until 20 F-waves were recorded.

2.4. Clinical symptom questionnaires

All patients completed questionnaires including duration of leg pain, type of pain (i.e. aching, shooting, stabbing), visual analogue scales for 'typical' and 'worse' pain (VAS; 0 – no pain, 10 – maximum pain), Hospital Anxiety and Depression Scale (HADS; 0 – no anxiety/depression, 21 – maximum anxiety/depression) and Oswestry Low Back Disability Questionnaire (ODI; 0, no disability; 100, maximum disability) and the Roland Morris Disability Questionnaire (RMDQ; 0, no disability; 24 maximum disability).

2.5. Data analysis

2.5.1. Diffusion Tensor Imaging (DTI)

Our previous work show that the DTI metrics derived from a healthy cohort between left and right sides and between vertebral levels are similar (Chiou et al., 2017). In the present study we therefore used the L4 nerve root (or S1 if there was evidence of compression at the L4 level) as a within-subject baseline measure in order to study the microstructural changes along the compressed L5 nerve root.

The post-processing of diffusion-weighted images (DWI) and fitting of the diffusion tensor were performed using the FSL Diffusion Toolbox (FDT) (FSL, http://fsl.fmrib.ox.ac.uk/fsl) v.5.0.6 (Oxford, UK). From the estimation of the diffusion tensor at each individual voxel, voxel-wise measures of mean Fractional Anisotropy (FA), Mean (MD), Axial (AD) and Radial (RD) Diffusivity were derived from respective Regions of Interest (ROI) along an affected (i.e. L5) and unaffected (i.e. L4 or S1) nerve. All ROIs were manually drawn by one person (author SWH) with reference to the axial view of b = 0 image from the diffusion acquisition overlaid onto the co-acquired axial T2-weighted image. Three binary ROIs were manually traced onto the image using FSLview (FSL, http://fsl.fmrib.ox.ac.uk/fsl) on either the L4 or S1 (unaffected) and L5 (affected) nerves at ~5 mm (i.e. proximal), ~12 mm (i.e. mid), and ~25 mm (i.e. distal) below the level of centre of the relevant disc (see Fig. 1). Each ROI volume was standardised across patients and drawn to cover the entire visible signal on the b = 0 image which was clearly differentiable as nerve, resulting in ROIs of between 40 and 60-mm^3. This size of ROI reduces the partial volume effect; the cross-sectional area of nerve roots in the lower lumbar region has been shown in a cadaveric study to be 34.48 ± 11.25 mm^2 (Inufusa et al., 1996).

2.5.2. EMG

The mean MEP amplitude per stimulus intensity was calculated and normalised to the M-max for each muscle. Mean pre-stimulus EMG was

Table 3
Relationship between FA, MD, AD and RD and the battery of clinical questionnaires. Results from Pearson correlation coefficient analyses between the diffusion metrics across all ROIs and clinical scores. AD: mean diffusivity, CMCT: central motor conduction time, FA, fractional anisotropy, ODI: Oswestry Low Back Disability Questionnaire, MD: mean diffusivity, RD: radial diffusivity, RMDQ: Roland Morris Disability Questionnaire, ROI: region of interest, VAS: visual analogue score. $N = 20$. * = significant correlation following correction for multiple comparisons using false detection rate (FDR).

Diffusion metric ROI	Anxiety	Depression	Average Leg Pain VAS	ODI	RMDQ
FA					
Proximal	r = −0.81	r = −0.31	r = 0.29	r = 0.11	r = −0.38
	p = 0.73	p = 0.19	p = 0.21	p = 0.63	p = 0.09
Mid	r = −0.31	r = −0.66	r = −0.05	r = −0.15	r = −0.27
	p = 0.19	p = 0.01*	p = 0.84	p = 0.52	p = 0.25
Distal	r = 0.08	r = 0.06	r = −0.51	r = −0.16	r = −0.17
	p = 0.73	p = 0.79	p = 0.02*	p = 0.49	p = 0.46
MD					
Proximal	r = 0.29	r = 0.41	r = 0.07	r = −0.04	r = 0.35
	p = 0.22	p = 0.07	p = 0.76	p = 0.85	p = 0.13
Mid	r = 0.13	r = 0.35	r = −0.98	r = −0.06	r = 0.20
	p = 0.58	p = 0.12	p = 0.68	p = 0.81	p = 0.41
Distal	r = 0.07	r = −0.04	r = 0.04	r = −0.15	r = −0.13
	p = 0.76	p = 0.85	p = 0.87	p = 0.53	p = 0.60
AD					
Proximal	r = 0.42	r = 0.46	r = 0.26	r = −0.02	r = 0.31
	p = 0.06	p = 0.04	p = 0.27	p = 0.94	p = 0.18
Mid	r = 0.11	r = 0.25	r = −0.04	r = −0.19	r = 0.09
	p = 0.65	p = 0.30	p = 0.87	p = 0.42	p = 0.68
Distal	r = 0.10	r = −0.06	r = −0.04	r = −0.27	r = −0.19
	p = 0.66	p = 0.80	p = 0.86	p = 0.25	p = 0.43
RD					
Proximal	r = 0.02	r = 0.17	r = −0.28	r = −0.25	r = 0.03
	p = 0.93	p = 0.48	p = 0.23	p = 0.30	p = 0.89
Mid	r = −0.09	r = 0.06	r = −0.12	r = 0.01	r = 0.04
	p = 0.67	p = 0.79	p = 0.96	p = 0.97	p = 0.86
Distal	r = 0.49	r = 0.19	r = 0.59	r = 0.32	r = 0.47
	p = 0.03*	p = 0.43	p = 0.01*	p = 0.17	p = 0.04*

calculated in a 100-ms window from the rectified EMG traces for the TA and soleus at each intensity. The average rectified EMG trace from the trials in which 120% AMT was delivered was used to derive the MEP latency for each muscle. The amplitude and latency of averaged M_{max} were measured and the minimum latency of F waves was identified from the recorded 20 F waves. Central motor conduction time (CMCT) and peripheral motor conduction time (PMCT) were calculated using the following equations:

$$\text{PMCT (ms)} = \frac{\text{Mmax latency+minimum F wave latency} - 1}{2}$$

$$CMCT\ (ms) = MEP\ latency - \left(\frac{M\max\ latency + min.F\ wave\ latency - 1}{2}\right)$$

2.6. Statistical analysis

All data were analysed using SPSS 23 (IBM Corp., Armonk, NY, USA) and Sigmaplot 12.5 (Systat Inc., USA) and were normally distributed as assessed using Shapiro-Wilk test. Two-way repeated measures (RM) ANOVA with Holm-Sidak multiple comparison post-hoc tests were used to investigate the relationship of the DTI parameters between ROI (i.e. proximal, mid and distal) and nerve root (i.e. affected L5 and unaffected L4 or S1). For all bilateral L5 patients ($n = 12$), the radiologically confirmed 'worst side' was used in the analysis. Within-subject comparisons were made between affected and unaffected nerve roots. To investigate the relationship between DTI parameters and neurophysiological measurements, multiple linear regression analyses were performed between diffusion values measured along affected and unaffected nerve roots and neurophysiological measurements from the TA muscle. Age, gender and body height were included as covariates of no interest. Pearson correlation coefficient analysis were also carried out between diffusion values measured along affected and unaffected nerve roots and clinical symptoms. Statistical significance was set at $p < 0.05$ and all data are presented as mean ± SD in the text and tables and mean ± SEM in the figures where appropriate. For correlation analysis, correction for multiple comparisons were made using false detection rate (FDR) within each of the independent conditions tested.

3. Results

3.1. Clinical characteristics

The most common cause of nerve root compression was facet joint hypertrophy (55%) at either the L4-L5 or L5-S1 levels. This caused impingement of transiting or exiting L5 nerve roots in the lateral recess or foramen, respectively. 20% of patients had stenosis as a result of degenerative changes in L4-L5 or L5-S1 discs, 15% had a combination of facet joint and ligamentum flavum hypertrophy at the L4-L5 level causing lateral recess stenosis and compression of the transiting L5 nerve root and 10% had compression of L5 nerve roots in the lateral recess at the L4-L5 level as a result of ligamentum flavum hypertrophy alone. The majority of patients presented with bilateral L5 nerve compression (60%), followed by left only (25%) and right only compression (15%). 65% of patients had intact S1 nerve roots, 20% had intact S1 and L4 nerve roots and 15% had intact L4 nerve roots.

3.2. Moderate to severe pain, functional impairment and mood changes in elderly patients with L5 nerve root compression

Self-reported leg pain symptoms showed that 'shooting' (30%) and 'ache' (30%) were the most common types of pain experienced (Table 1). The least common type of pain was described as 'sharp' (15%) and 25% of patients reported experiencing more than one type of pain (e.g. sharp/shooting, stabbing/shooting, ache/stabbing, ache/sharp, burning/sharp). The most commonly reported duration of leg pain was between 1 and 4 years (35%) with 30% experiencing leg pain for between 5 and 10 years, 15% for 1 year, 15% for > 10 years and 5% for 6 months. The average leg pain VAS reported was 7.24 ± 1.47.

3.3. Changes in microstructural integrity along compressed L5 nerve roots

We have previously demonstrated that DTI metrics are similar between left and right sides and between vertebral levels in healthy, pain-free subjects (Chiou et al., 2017). Therefore, within-subject comparisons between radiologically confirmed affected (i.e. L5 nerve root) and unaffected (i.e. L4 or S1 nerve root) vertebral levels were used in the analysis. DTI showed a difference in the microstructural integrity along affected versus unaffected nerves (Fig. 2). Two-way repeated measures ANOVA revealed that there was a main effect of Nerve (i.e. between affected and unaffected nerves: $F_{1,19} = 5.34$, $p < 0.05$) and ROI ($F_{2,38} = 11.03$, $p < 0.001$) on FA. The differences in FA were prominent in the proximal ROIs and although there was no interaction between ROI and Nerve, there was a statistical trend ($F_{2,38} = 3.01$, $p = 0.06$).

Fig. 2B – D show the changes in MD, AD and RD were localised to the proximal segment of the compressed nerve root. There was an interaction between ROI and nerve (MD: $F_{2,38} = 6.69$, $p < 0.01$; AD: $F_{2,38} = 4.65$, $p < 0.01$; RD: $F_{2,38} = 7.03$, $p < 0.01$) and for each of these measures, this effect was driven by differences in the proximal part of the affected nerve (MD: $t(19) = 3.12$, $p < 0.01$; AD: $t(19) = 2.74$, $p < 0.01$; RD $t(19) = 3.93$, $p < 0.001$), but not in the mid (MD: $t(19) = 0.71$, $p = 0.48$; AD: $t(19) = 0.23$, $p = 0.79$; RD: $t(19) = 0.42$, $p = 0.42$) or distal (MD: $t(19) = 0.45$, $p = 0.65$; AD: t

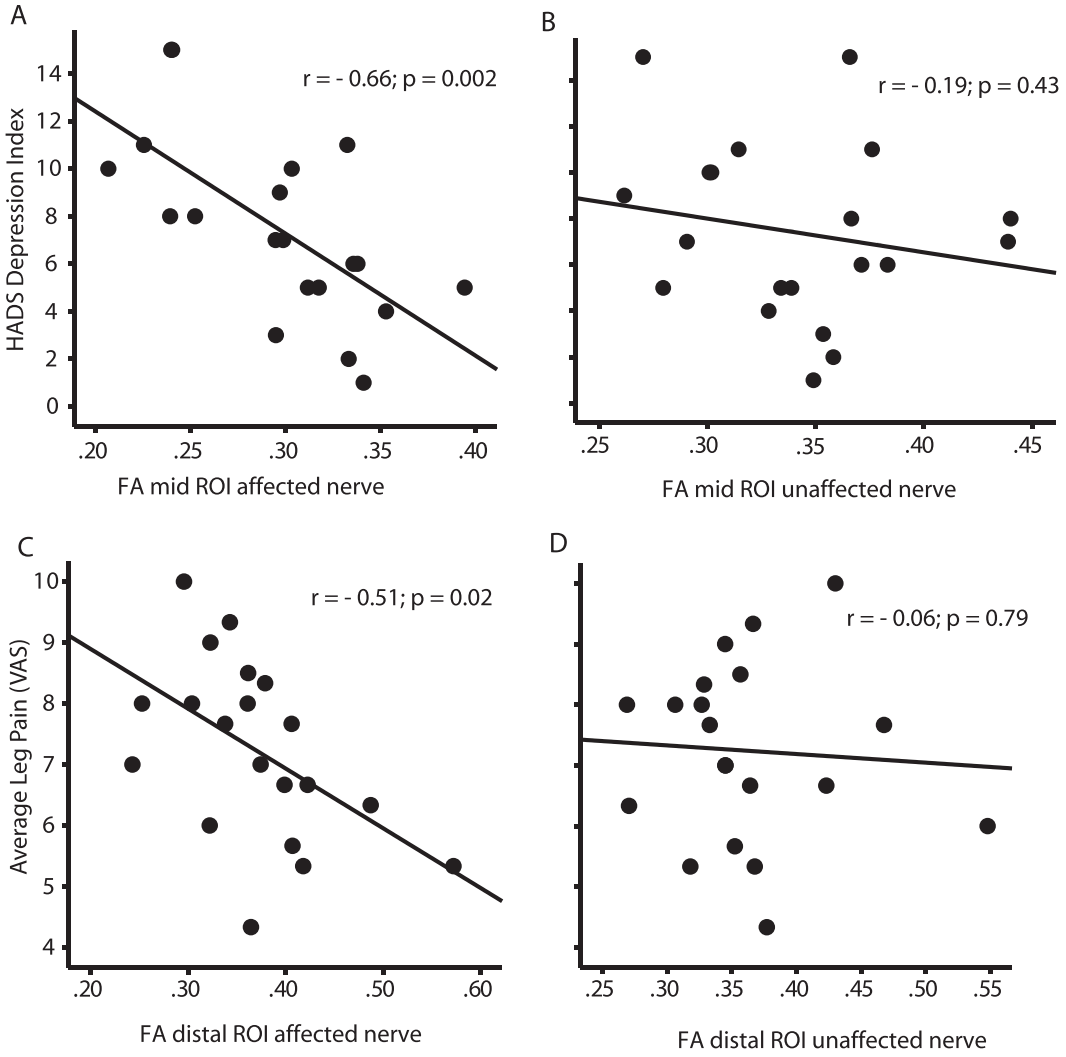

Fig. 4. Relationship between fractional anisotropy (FA) measured along affected and unaffected nerve roots and chronic pain symptoms. A) FA measured from the mid-part of the affected nerve correlated with HADS depression score which was not seen for the unaffected nerve root (B). FA measured at a distal part of the compressed nerve correlated with self-rated average pain visual analogue scale (VAS) score (C) which was not seen for the unaffected nerve root (D). N = 20.

(19) = 0.42, p = r0.67; RD: t(19) = 0.04, p = 0.9) segments.

3.4. Correlation between diffusion metrics derived along compressed nerve roots and motor neurophysiological responses

The relationship between FA measured along the compressed nerve roots and the battery of neurophysiological tests were analysed. There were no significant correlations between FA measured at proximal and distal parts of the nerve and any of the neurophysiological assessments (see Table 2). However, significant correlations were found between FA measured at the mid part of the nerve and minimum F-wave latencies ($r = -0.54$; $p < 0.05$; Fig. 3A) and peripheral motor conduction time (PMCT: $r = -0.43$; p < 0.05; Fig. 3C) in the affected nerve root but not at the same position in the unaffected nerve root (min F-wave latencies: $r = 0.09$; $p = 0.71$; PMCT: $r = 0.16$; $p = 0.53$; Fig. 3B and D).

For MD, AD and RD metrics, there were no significant correlations between any of the diffusion values measured at the proximal or mid parts of the nerve, however there was a correlation between MD measured at the distal ROI and MEP amplitude in the affected nerve root ($r = -0.61$; $P < 0.05$; Table 2).

3.5. Correlation between diffusion metrics derived along compressed nerve roots and clinical scores

Table 3 shows the correlations between all diffusion metrics and clinical measures. HADS depression score correlated with FA measured at the mid part of the affected ($r = -0.66$; $p < 0.01$; Fig. 4A) but not the unaffected ($r = -0.19$; $p = 0.43$; Fig. 4B) nerve root. The average leg pain score correlated with FA measured at the distal part of the affected ($r = -0.51$; $p < 0.05$; Fig. 4C) but not the unaffected ($r = -0.06$; $p = 0.79$; Fig. 4D) nerve root. In addition, HADS depression score correlated with AD measured at the proximal part of the affected ($r = 0.46$; p < 0.05; Table 3) but not the unaffected nerve root ($r = 0.24$; $p = 0.31$). There was also a significant correlation between the anxiety, average leg pain and the RMDQ scores and RD measured at the distal part of the affected (anxiety: $r = 0.49$; p < 0.05; leg pain: $r = 0.59$; p < 0.01; RMDQ: $r = 0.47$; p < 0.05; Table 3) but not the unaffected nerve roots (anxiety: $r = -0.23$; $p = 0.33$; leg pain: $r = 0.19$; p = 0.43; RMDQ: $r = -0.32$; $p = 0.172$).

4. Discussion

In this study, we have explored the use of DTI to measure microstructural integrity along compressed (i.e. L5) or intact (i.e. L4 or S1)

nerve roots in elderly stenosis patients and investigated relationships to a battery of neurophysiological measures of motor function and clinical symptoms associated with chronic pain. We show that FA was lower in compressed L5 nerves compared to an unaffected L4 or S1 nerve root. The diffusion metrics MD, AD and RD were elevated at the proximal end of compressed nerve roots compared to an unaffected level. These results indicate that DTI can be used to quantify the microstructural integrity along compressed nerve roots in elderly patients with stenosis. Further, we have shown that diffusion values measured along compressed L5 nerve roots appear to relate closely with a battery of clinical symptoms associated with chronic pain and is therefore a promising way to stratify treatment selection and to predict outcomes.

Critically, we have shown that DTI can be used to objectively measure nerve root compression. Conventional imaging techniques such as MRI, CT and radiography can provide effective means of evaluating the extent of narrowing within the exit foramen (Hasegawa et al., 1995; Kirkaldy-Willis et al., 1982; Vanderlinden, 1984). However, these imaging techniques do not often provide enough evidence alone to predict who will respond to a particular treatment. We have shown that through using DTI it is possible to provide a detailed quantifiable evaluation of spinal nerve root entrapment. DTI therefore has the added benefit of being able to diagnose a neuropathy (Eguchi et al., 2016a, Kanamoto et al., 2016, Kitamura et al., 2012) and we have highlighted how this technique offers insight into the pathological processes associated with this condition.

We have previously shown in healthy subjects that the diffusion values measured between sides and levels along nerve roots in the lumbar and sacral regions of the spinal cord are comparable (Chiou et al., 2017). In this study, we have shown that it is possible to measure pathological changes in diffusion parameters in compressed nerve roots that can be compared to normative values measured from an unaffected level, which is in line with previous reports (Balbi et al., 2011; Eguchi et al., 2016b; Eguchi et al., 2010). Interestingly, we found relationships between neurophysiological measures and clinical scores only in the affected nerve roots.

We found relationships between the degree of L5 nerve root compression and a number of neurophysiological measures from the TA muscle. This not only provides insight into the relationship with the development of motor deficiencies but also to the underlying pathophysiology of the affected nerve root. Neurophysiological assessments are typically used in nerve entrapment disorders as a means to detect the location and severity of the compression (Kane and Oware, 2012). The initial lesion is typically a focal damage to myelin sheath which is reflected in the slowing of nerve conduction at the site of compression (Whittaker, 2012). Here, we show that FA measured along compressed nerve roots correlated with neurophysiological tests of minimum F-wave latency and PMCT. A recent neurophysiological study assessing median nerve structural integrity and function in healthy volunteers suggests that FA, in part, reflects myelin sheath integrity (Heckel et al., 2015). Further, our previous research has demonstrated that FA is sensitive to the inherent variance observed in functional neurophysiological parameters that relate the spinal nerve integrity in healthy volunteers (Chiou et al., 2017). It is therefore feasible that FA values derived from compressed nerve roots in the exit foramen are sensitive to the focal damage to myelin sheath associated with the nerve entrapment. Our data suggest that pathological FA values may serve as a biomarker of demyelination at the site of nerve compression. Therefore, using specific DTI parameters to investigate nerve root compression provides a novel means by which to identify neuropathy and may give insight into whether a nerve lesion is predominantly axonal or demyelinating.

In this study we have shown detailed analysis of the microstructural integrity along compressed nerve roots through evaluating RD and AD, which refer to diffusivity parallel and perpendicular to the nerve fibre orientation, respectively and MD which reflects changes in both RD and AD. There were significant pathological changes in AD, RD and MD at the proximal end of the compressed nerve roots suggesting changes in axonal integrity, myelin sheath integrity and intra-neural oedema, respectively (Song et al., 2003; Song et al., 2002; Heckel et al., 2015; Eguchi et al., 2016b; Eguchi et al., 2016a; Khalil et al., 2008). Interestingly, these changes in nerve root integrity appear to be localised to the proximal end of the compressed nerve root which is line with previous studies (Eguchi et al., 2016b, Eguchi et al., 2010) and we did not see pathological changes at mid or distal parts of the nerve. Other studies have shown that AD, RD and MD are less sensitive than FA for detecting microstructural changes in compressed nerve roots and it is therefore possible that these measures have failed to detect a change in nerve microstructural integrity at more distal regions of the nerve (Balbi et al., 2011; Eguchi et al., 2010). In line with this, a recent study demonstrated that FA showed a higher accuracy than MD in distal regions along the nerve root (Eguchi et al., 2016b). It is also possible that chronic nerve root compression may result in localised changes in the microstructural integrity within the anterior part of the nerve due to a series of inflammatory and degenerative changes (Kobayashi et al., 2004).

In this study, we also found relationships between nerve compression and distinct clinical symptoms related to chronic pain. Structured neurological examinations are typically recommended during the clinical decision making process in the management of nerve compression syndromes (Kane and Oware, 2012). However, these measures correlate poorly with the level of disability and patients' reported symptoms (Mondelli et al., 2000; Longstaff et al., 2001). In the present study, we show a direct relationship between diffusion metrics values measured along compressed L5 nerve roots and patients' self-rated clinical symptoms. In contrast, correlations were not found with the respective unaffected nerve roots. This highlights that DTI can reveal selective damage to specific nerve roots and how this manifests as distinct clinical symptoms. Previous research examining the relationship between conventional MR imaging and symptoms suggest that the relationship between spinal pathology and pain is unclear and that only severe pathology is associated with the development of clinical symptoms (Geisser et al., 2007). Others have also demonstrated that the degree of stenosis did not correspond to changes in clinical scores (Amundsen et al., 1995) suggesting patients' symptoms may be determined by a number of other underlying factors. Using advanced neuroimaging, such as that presented here, provides a means by which to measure changes in nerve microstructural integrity; changes which manifest as the development of chronic pain and associated co-morbidities. The findings from this study suggest that DTI of compressed nerve roots may serve as a predictor of pain severity and the development of associated affective disorders in elderly stenosis patients.

The present study suggests that it may be possible to stratify elderly patients with stenosis based on degree of nerve root compression. It is apparent that relationships hold between the extent of nerve compression and pain severity as well as other co-morbidities such as anxiety, depression and disability rating. It is feasible that this information can be used as part of a biopsychosocial screening tool to stratify patients into prognostic subgroups (Bernstein et al., 2017); classification of patients based on anatomy, pathology, pain mechanisms or psychosocial factors has the potential to allow more targeted treatment based on underlying mechanisms (O'sullivan, 2005; Vollert et al., 2016). A similar framework has been shown to be effective in targeting specific treatments to patients with chronic low back pain where there is a similarly large degree of heterogeneity in signs, symptoms and underlying mechanisms (O'sullivan, 2005). Using DTI, it may be possible to use the values of diffusion parameters to separate patients and generate predictive models of treatment outcomes (e.g. based on pain scales) based on inherent patterns in the data. Such phenotype-stratification would be key in providing additional information for diagnosis, treatment and, importantly, predictions to be made about treatment outcomes.

It should be noted that there are difficulties associated with

acquisition of high-quality DTI in the lumbar spine, due to the close relationships of the nerves to osseous and ligamentous structures. However, we have mitigated against these during the development of the sequences and the processing pipelines used, which were built upon previous methods to image lumbar spinal nerves. We are confident that we have accounted for problems associated with imaging at the interface between bone and neural tissue as we were able to show differences in DTI metrics between unaffected and affected nerves, which is in accordance with previously published work using DTI in the lumbar spine (Eguchi et al., 2016b).

In summary, the present study demonstrates the clinical application of DTI in the assessment of nerve root compression and determined relationships to clinical symptoms associated with chronic pain and motor deficiencies in elderly foraminal stenosis patients. We have shown that DTI can be used to quantify nerve microstructural integrity in compressed nerve roots which relate to chronic pain and co-morbidities such as anxiety, depression and functional impairment. Taken together, this study indicates that it may be possible to use DTI to identify foraminal nerve root compression and provide quantifiable information relating to the degree of nerve injury. Further, these data provide a rationale for the use of DTI to stratify treatment selection and to track improvements or predict outcomes following decompression surgery.

Declarations of interest

None.

Funding

This work was supported by Dunhill Medical Trust (grant number R401/0215).

References

Amundsen, T., Weber, H., Lilleas, F., Nordal, H.J., Abdelnoor, M., Magnaes, B., 1995. Lumbar spinal stenosis. In: Clinical and Radiologic Features. 20. pp. 1178–1186 Spine (Phila Pa 1976).
Balbi, V., Budzik, J.F., duhamel, A., bera-louville, A., Le Thuc, V., Cotten, A., 2011. Tractography of lumbar nerve roots: initial results. Eur. Radiol. 21, 1153–1159.
Bernstein, I.A., Malik, Q., Carville, S., Ward, S., 2017. Low back pain and sciatica: summary of NICE guidance. BMJ 356, i6748.
Chiou, S.Y., Hellyer, P.J., Sharp, D.J., Newbould, R.D., Patel, M.C., Strutton, P.H., 2017. Relationships between the integrity and function of lumbar nerve roots as assessed by diffusion tensor imaging and neurophysiology. Neuroradiology 59, 893–903.
Eguchi, Y., Ohtori, S., Yamashita, M., Yamauchi, K., Suzuki, M., Orita, S., Kamoda, H., Arai, G., Ishikawa, T., Miyagi, M., Ochiai, N., Kishida, S., Masuda, Y., Ochi, S., Kikawa, T., Takaso, M., Aoki, Y., Toyone, T., Suzuki, T., Takahashi, K., 2010. Clinical applications of diffusion magnetic resonance imaging of the lumbar foraminal nerve root entrapment. Eur. Spine J. 19, 1874–1882.
Eguchi, Y., Ohtori, S., Orita, S., Kamoda, H., Arai, G., Ishikawa, T., Miyagi, M., Inoue, G., Suzuki, M., Masuda, Y., Andou, H., Takaso, M., Aoki, Y., Toyone, T., Watanabe, A., Takahashi, K., 2011. Quantitative evaluation and visualization of lumbar foraminal nerve root entrapment by using diffusion tensor imaging: preliminary results. AJNR Am. J. Neuroradiol. 32, 1824–1829.
Eguchi, Y., Ohtori, S., Suzuki, M., Oikawa, Y., Yamanaka, H., Tamai, H., Kobayashi, T., Orita, S., Yamauchi, K., Suzuki, M., Aoki, Y., Watanabe, A., Kanamoto, H., Takahashi, K., 2016a. Diagnosis of lumbar Foraminal stenosis using diffusion tensor imaging. Asian Spine J. 10, 164–169.
Eguchi, Y., Ohtori, S., Suzuki, M., Oikawa, Y., Yamanaka, H., Tamai, H., Kobayashi, T., Orita, S., Yamauchi, K., Suzuki, M., Aoki, Y., Watanabe, A., Kanamoto, H., Takahashi, K., 2016b. Discrimination between lumbar Intraspinal stenosis and Foraminal stenosis using diffusion tensor imaging parameters: preliminary results. Asian Spine J. 10, 327–334.
El Barzouhi, A., Verwoerd, A.J., Peul, W.C., Verhagen, A.P., Lycklama, A.N.G.J., van der Kallen, B.F., Koes, B.W., Vleggeert-Lankamp, C.L., Leiden-The Hague Spine Intervention Prognostic Study, G, 2016. Prognostic value of magnetic resonance imaging findings in patients with sciatica. J. Neurosurg. Spine 24, 978–985.
Geisser, M.E., Haig, A.J., Tong, H.C., Yamakawa, K.S., Quint, D.J., Hoff, J.T., Miner, J.A., Phalke, V.V., 2007. Spinal canal size and clinical symptoms among persons diagnosed with lumbar spinal stenosis. Clin. J. Pain 23, 780–785.
Hasegawa, T., AN, H.S., Haughton, V.M., Nowicki, B.H., 1995. Lumbar foraminal stenosis: critical heights of the intervertebral discs and foramina. A cryomicrotome study in cadavera. J. Bone Joint Surg. Am. 77, 32–38.
Heckel, A., Weiler, M., Xia, A., Ruetters, M., Pham, M., Bendszus, M., Heiland, S., Baeumer, P., 2015. Peripheral nerve diffusion tensor imaging: assessment of axon and myelin sheath integrity. PLoS ONE 10, e0130833.
Hellyer, P.J., Leech, R., Ham, T.E., Bonnelle, V., Sharp, D.J., 2013. Individual prediction of white matter injury following traumatic brain injury. Ann. Neurol. 73, 489–499.
Hess, C.W., Mills, K.R., Murray, N.M., 1987. Responses in small hand muscles from magnetic stimulation of the human brain. J. Physiol. 388, 397–419.
Inufusa, A., An, H.S., Lim, T.H., Hasegawa, T., Haughton, V.M., Nowicki, B.H., 1996. Anatomic changes of the spinal canal and intervertebral foramen associated with flexion-extension movement. Spine (Phila Pa 1976) 21, 2412–2420.
Kalichman, L., Cole, R., Kim, D.H., Li, L., Suri, P., Guermazi, A., Hunter, D.J., 2009. Spinal stenosis prevalence and association with symptoms: the Framingham study. Spine J. 9, 545–550.
Kanamoto, H., Eguchi, Y., Suzuki, M., Oikawa, Y., Yamanaka, H., Tamai, H., Kobayashi, T., Orita, S., Yamauchi, K., Suzuki, M., Aoki, Y., Watanabe, A., Takahashi, K., Ohtori, S., 2016. The diagnosis of double-crush lesion in the L5 lumbar nerve using diffusion tensor imaging. Spine J. 16, 315–321.
Kane, N.M., Oware, A., 2012. Nerve conduction and electromyography studies. J. Neurol. 259, 1502–1508.
Khalil, C., Hancart, C., Le Thuc, V., Chantelot, C., Chechin, D., Cotten, A., 2008. Diffusion tensor imaging and tractography of the median nerve in carpal tunnel syndrome: preliminary results. Eur. Radiol. 18, 2283–2291.
Kirkaldy-Willis, W.H., Wedge, J.H., Yong-Hing, K., Tchang, S., de Korompay, V., Shannon, R., 1982. Lumbar spinal nerve lateral entrapment. Clin. Orthop. Relat. Res. 171–178.
Kitamura, M., Eguchi, Y., Inoue, G., Orita, S., Takaso, M., Ochiai, N., Kishida, S., Kuniyoshi, K., Aoki, Y., Nakamura, J., Ishikawa, T., Arai, G., Miyagi, M., Kamoda, H., Suzuki, M., Furuya, T., Toyone, T., Takahashi, K., Ohtori, S., 2012. A case of symptomatic extra-foraminal lumbosacral stenosis ("far-out syndrome") diagnosed by diffusion tensor imaging. Spine (Phila Pa 1976) 37, E854–E857.
Kobayashi, S., Yoshizawa, H., Yamada, S., 2004. Pathology of lumbar nerve root compression. Part 1: Intraradicular inflammatory changes induced by mechanical compression. J. Orthop. Res. 22, 170–179.
Longstaff, L., Milner, R.H., O'sullivan, S., Fawcett, P., 2001. Carpal tunnel syndrome: the correlation between outcome, symptoms and nerve conduction study findings. J. Hand Surg. (Br.) 26, 475–480.
Melancia, J.L., Francisco, A.F., Antunes, J.L., 2014. Spinal stenosis. Handb. Clin. Neurol. 119, 541–549.
Mondelli, M., Reale, F., Sicurelli, F., Padua, L., 2000. Relationship between the self-administered Boston questionnaire and electrophysiological findings in follow-up of surgically-treated carpal tunnel syndrome. J. Hand Surg. (Br.) 25, 128–134.
Nagy, Z., Weiskopf, N., 2008. Efficient fat suppression by slice-selection gradient reversal in twice-refocused diffusion encoding. Magn. Reson. Med. 60, 1256–1260.
NICE, 2016. Spinal Injury: Assessment and Initial Management.
Nicotra, A., King, N.K., Catley, M., Mendoza, N., Mcgregor, A.H., Strutton, P.H., 2013. Evaluation of corticospinal excitability in cervical myelopathy, before and after surgery, with transcranial magnetic stimulation: a pilot study. Eur. Spine J. 22, 189–196.
Oikawa, Y., Eguchi, Y., Inoue, G., Yamauchi, K., Orita, S., Kamoda, H., Ishikawa, T., Miyagi, M., Suzuki, M., Sakuma, Y., Kubota, G., Inage, K., Saino, T., Sato, H., Ando, H., Kojima, M., Okumura, K., Masuda, Y., Watanabe, A., Takahashi, K., Ohtori, S., 2015. Diffusion tensor imaging of lumbar spinal nerve in subjects with degenerative lumbar disorders. Magn. Reson. Imaging 33, 956–961.
Orita, S., Inage, K., Eguchi, Y., Kubota, G., Aoki, Y., Nakamura, J., Matsuura, Y., Furuya, T., Koda, M., Ohtori, S., 2016. Lumbar foraminal stenosis, the hidden stenosis including at L5/S1. Eur. J. Orthop. Surg. Traumatol. 26, 685–693.
O'sullivan, P., 2005. Diagnosis and classification of chronic low back pain disorders: maladaptive movement and motor control impairments as underlying mechanism. Man. Ther. 10, 242–255.
Rossi, S., Hallett, M., Rossini, P.M., Pascual-Leone, A., 2011. Screening questionnaire before TMS: an update. Clin. Neurophysiol. 122, 1686.
Rydevik, B., Brown, M.D., Lundborg, G., 1984. Pathoanatomy and pathophysiology of nerve root compression. Spine (Phila Pa 1976) 9, 7–15.
Rydevik, B.L., Pedowitz, R.A., Hargens, A.R., Swenson, M.R., Myers, R.R., Garfin, S.R., 1991. Effects of acute, graded compression on spinal nerve root function and structure. An experimental study of the pig cauda equina. Spine (Phila Pa 1976) 16, 487–493.
Sharp, D.J., Scott, G., Leech, R., 2014. Network dysfunction after traumatic brain injury. Nat. Rev. Neurol. 10, 156–166.
Song, S.K., Sun, S.W., Ramsbottom, M.J., Chang, C., Russell, J., Cross, A.H., 2002. Dysmyelination revealed through MRI as increased radial (but unchanged axial) diffusion of water. Neuroimage 17, 1429–1436.
Song, S.K., Sun, S.W., Ju, W.K., Lin, S.J., Cross, A.H., Neufeld, A.H., 2003. Diffusion tensor imaging detects and differentiates axon and myelin degeneration in mouse optic nerve after retinal ischemia. Neuroimage 20, 1714–1722.
Takahashi, N., Yabuki, S., Aoki, Y., Kikuchi, S., 2003. Pathomechanisms of nerve root injury caused by disc herniation: an experimental study of mechanical compression and chemical irritation. Spine (Phila Pa 1976) 28, 435–441.
Vanderlinden, R.G., 1984. Subarticular entrapment of the dorsal root ganglion as a cause of sciatic pain. Spine (Phila Pa 1976) 9, 19–22.
Verwoerd, A.J., Luijsterburg, P.A., Lin, C.W., Jacobs, W.C., Koes, B.W., Verhagen, A.P., 2013. Systematic review of prognostic factors predicting outcome in non-surgically treated patients with sciatica. Eur. J. Pain 17, 1126–1137.
Vollert, J., Attal, N., Baron, R., Freynhagen, R., Haanpaa, M., Hansson, P., Jensen, T.S., Rice, A.S., Segerdahl, M., Serra, J., Sindrup, S.H., Tolle, T.R., Treede, R.D., Maier, C., 2016. Quantitative sensory testing using DFNS protocol in Europe: an evaluation of heterogeneity across multiple centers in patients with peripheral neuropathic pain and healthy subjects. Pain 157, 750–758.
Whittaker, R.G., 2012. The fundamentals of electromyography. Pract. Neurol. 12, 187–194.